Electrophoresis in Protein Crystal: Nonequilibrium Molecular Dynamics Simulations

Zhongqiao Hu and Jianwen Jiang
Department of Chemical and Biomolecular Engineering, National University of Singapore, Singapore 117576

ABSTRACT Electrophoresis of a mixture of NaCl and $CaCl_2$ in a lysozyme crystal is investigated using nonequilibrium molecular dynamics (MD) simulations. Upon exposure to an electric field, the stability of lysozyme is found to decrease slightly. This finding is demonstrated by increases in the root mean-square deviations of the heavy atoms of lysozyme, in the solvent-accessible surface area of hydrophobic residues, and in the number of hydrogen bonds between lysozyme and water. The solvent-accessible surface area of hydrophilic residues changes marginally, and the number of hydrogen bonds between lysozyme molecules decreases. Water molecules tend to align preferentially parallel to the electric field, and the dipole moment along the pore axis increases linearly with increasing field strength. Two pronounced layered structures are observed for Na^+ and Ca^{2+} in the vicinity of protein surface, but only one enriched layer is observed for Cl^-. The number distributions of all ions are nearly independent of the electric field. The water coordination numbers of all ions are smaller in the crystal than in aqueous bulk solution; however, the reverse is found for the Cl^- coordination numbers of cations. Both the water and the Cl^- coordination numbers are insensitive to the electric field. Ion diffusivities in the crystal are ~2 orders of magnitude smaller than those in aqueous bulk solution. The drift velocities of ions increase proportionally to the electric field, particularly at high strengths, and depend on ionic charge and coordination with oppositely charged ions. Electrical current exhibits a linear relationship with the field strength. The zero-field electrical conductivity is estimated to be 0.56 S/m, which is very close to 0.61 S/m as predicted by the Nernst-Einstein equation.

INTRODUCTION

Electrophoresis refers to the transport or migration of ions under the influence of an electric field and is of central importance in separation, sensing, biology, etc. For instance, capillary electrophoresis is a commonly used method for the purification of ionic species in buffer-filled narrow capillaries that are 25–100 μm in diameter (1). A recent study showed that DNA adsorbed on a nanopatterned surface had a length-dependent mobility under an electric field and thus was separated. This finding enabled a new method for the rational design of nanodevices using surface-directed separation (2). In cell membranes, there is an instantaneous electric field between intra- and extracellular environments that drives ions and pharmaceutical molecules across membranes in many bioprocesses (3). As a consequence, a better understanding of electrophoresis in confined space is of central importance to the development of new approaches to engineering controllable nanofluidic channels and to fine-tuning lap-on-a-chip devices and biologically significant electrical signaling in nervous systems.

For decades, the Poisson-Nernst-Planck (PNP) model has been used to describe electrophoresis (4). The mean field-based PNP model provides a classical continuum framework, but it does not incorporate molecular level details and correlations. As a result, the PNP model cannot be used to examine the complexity of electrophoresis, particularly at the molecular scale, because the confined channel is in the nanodomain, the surface/volume ratio is large, and the interfacial effect dominates. Alternatively, molecular simulations with their ever-growing computational power have been increasingly used because of their ability to provide microscopic insights that are otherwise experimentally inaccessible or difficult to obtain. Tang et al. (5,6) conducted molecular dynamics (MD) simulations to investigate the effects of confinement on the structural and transport properties of 0.5 M KCl in cylindrical nanopores of radii 4.75–15.8 Å. Their results demonstrated that a decrease in the hydration of ions and hydrogen bonding of water occurs as pore radius decreases and that the external electric field has a strong influence on the orientation of water molecules. Dzubiella et al. (7,8) reported results of an MD simulation study on electric field-controlled water permeation coupled to ion transport through a hydrophobic nanopore. Their results suggested that an ionic charge imbalance across the nanopore induces water permeation and thus ionic permeability. Murad et al. (9,10) used MD simulations to study the separation of supercritical aqueous electrolyte solutions in thin zeolite membranes. They found the important role of the electric field in enhancing the separation rate and demonstrated the serious risk of applying macroscopic hydrodynamics to nanoscale systems. Hwang et al. (11,12) developed a kinetic lattice grand canonical Monte Carlo simulation method for a model ion channel system. Their results showed that simulated ion currents, electrostatic potentials, and ion concentrations agree well with the PNP predictions if the channel has the same dielectric constant as water; however, there is considerable difference if the channel has a lower dielectric constant and so the reaction field effect is missing in PNP theory (11,12).

Submitted June 15, 2008, and accepted for publication July 8, 2008.

Address reprint requests to Jianwen Jiang, Dept. of Chemical and Biomolecular Engineering, National University of Singapore, Singapore 117576. E-mail: chejj@nus.edu.sg.

Editor: Ron Elber.

0006-3495/08/11/4148/09 $2.00

doi: 10.1529/biophysj.108.140160

The electric field may enhance conductivity and permeability of molecules in biomembranes. This enhancement can trigger drug delivery across cell membranes (electroporation) and be used for cancer treatment and gene therapy (13). However, understanding the fundamental mechanism of transport in biomembranes is difficult on a microscopic scale due to the unknown atomic structures of many membrane proteins, which are not easily crystallized. Recently, it has been recognized that protein crystals can serve as a remarkable benchmark for biomembranes because of the biological similarity between the pores in protein crystals and the channels in biomembranes; also, importantly, the structures of a large number of proteins are readily available (14). Therefore, the study of fluid behavior in protein crystals under an electric field is significant, because it can provide insight into the less easily observed behavior in biomembranes. With high porosities, large surface areas, a wide range of pore sizes, and unique chiral environments, protein crystals have also emerged as new separation media for chemically or optically different molecules through size exclusion or chiral discrimination (15). Water and ions are ubiquitously involved in separation processes, and a better understanding of their behavior from a molecular level is of central importance for the rational design of high-performance bioseparation technologies.

Previously, we reported an equilibrium MD (EMD) simulation study to investigate the spatial and temporal properties of ions and water in three protein crystals with different morphologies and topologies. The mobility in the crystals was found to be anisotropic preferentially along the pore axis and to be enhanced with increasing porosity (16). In this work, nonequilibrium MD (NEMD) simulations were performed to explore electrophoresis in a lysozyme crystal under the electric field. The NEMD method was first proposed by Evans and Morris (17) and later applied to bulk electrolytes (18). We chose lysozyme as a model protein because it is readily available and has a well-known structure. Lysozyme functions to kill bacteria and is commonly regarded as the body's own antibiotic. An electrolyte mixture of NaCl and $CaCl_2$ is thought to represent a general buffer solution. In addition to the static and transport properties of Na^+, Ca^{2+}, and Cl^- ions, we examined the orientation of water molecules and the stability of lysozyme molecules under the electric field. Water plays a critical role in the structure, dynamics, and functionality of proteins; a clear understanding of confined water in protein crystal is of fundamental interest. It is also intriguing to study the stability and the structural change of protein under the electric field, which have rarely been examined. This is an important topic because an increasingly greater number of electrical devices are used around us daily.

MODEL AND METHOD

Lysozyme can exist in different crystalline forms, namely, tetragonal, orthorhombic, monoclinic and triclinic (19). In this work, tetragonal lysozyme (Protein Data Bank ID: 1HEL) is considered with a $P4_32_12$ space group (20). The lattice constants are $a = 7.91$ nm, $b = 7.91$ nm, and $c = 3.79$ nm. Fig. 1 shows a unit cell of tetragonal lysozyme crystal on the xy plane. The secondary structures (α-helices, β-sheets, and random coils) are indicated in Fig. 1 *a*. The formation of the secondary structures in protein molecules is attributed to the relatively stronger hydrogen bonding; consequently, the residues forming the secondary structures exhibit less mobility (16). Fig. 1 *b* shows the surface representations of the hydrophobic and hydrophilic resides. In the crystal, biological nanopores are periodically distributed with different sizes and shapes and are interconnected. Among them are two major pores in a unit cell; one is at the center and the other at the corner, which is shown clearly in Fig. 1. The major pore is approximately cylindrical along the z axis with a slight zigzag, and the radius is in the range of 0.6–0.7 nm (16).

The simulation box contained two unit cells with a size of $7.91 \times 7.91 \times 7.58\ nm^3$. At the physiological condition (pH $\approx$ 7), Arg and Lys residues were protonated, whereas Asp and Glu residues were deprotonated based on the experimental pK_a (21). As a consequence, each lysozyme molecule carried eight positive unit charges. Water molecules were added to mimic a fully hydrated crystal and three types of ions (Cl^-, Na^+, and Ca^{2+}) were introduced randomly while the system was kept neutral. Finally, the simulation box consisted of 16 lysozyme molecules, 5270 water molecules, 557 Cl^- ions (1.95 M), 143 Na^+ ions (0.50 M), and 143 Ca^{2+} ions (0.50 M). The GROMOS96 united-atom force field was adopted for lysozyme and ions (22). Water was mimicked by the simple point charge model (23). The pairwise nonbonded interactions consisted of Lennard-Jones (LJ) and Coulombic potentials. Table 1 provides the LJ parameters and charges of the three ions and water atoms. The periodic boundary conditions were exerted in all three dimensions to mimic an infinitely large crystal structure. A cutoff of 1.4 nm was used to evaluate the LJ interactions. The long-range electrostatic interactions were evaluated using the particle-mesh Ewald method with a grid spacing of 0.12 nm and the fourth-order interpolation. The bond lengths with dangling hydrogen atoms in lysozyme molecules were constrained using the LINCS algorithm, whereas H_2O geometry was constrained using the SETTLE algorithm.

Simulations were performed with the GROMACS v.3.3.1 package because it is extremely fast and particularly well-suited for biomolecular systems (24). The system was initially subject to energy minimization using the steepest descent method with a maximum step size of 0.01 nm and a force tolerance of 10 kJ mol^{-1} nm^{-1}. Then velocities were assigned according to the Maxwell-Boltzmann distribution at 300 K, followed by a 2 ns MD simulation. Drift velocities were tracked by an NEMD simulation to ensure the system reached a steady state. In the absence of an electric field, an EMD simulation was run, with energy monitored to ensure the system reached equilibrium. Finally, 10 ns MD simulations were conducted for production. MD simulations were performed in a canonical ensemble (NVT) at 300 K using the Berendsen thermostat with a relaxation time of 0.1 ps. An integration time step of 2 fs was used, and trajectories were saved every 1 ps.

For the NEMD simulation in this study, a uniform electric field was exerted along the nanopore axis (the z direction) ranging from $E_z = 0.1, 0.2, 0.3,$ to 0.4 V/nm. It should be noted that the electric field strength adopted in this study is typically 1 to 2 orders of magnitude stronger than that across cell membranes or used experimentally (25,26). Such a strong electric field is commonly used in molecular simulation to reduce the impact of thermal noise and therefore to enhance the signal/noise ratio within a nanosecond timescale (7). Furthermore, it is a delicate matter to maintain the temperature in NEMD simulations, because the ohmic heat generated by ion flux under the electric field must be removed (27). To calculate the temperature in NEMD runs, the ion velocities along the direction of the electric field were subtracted. In our NEMD simulation, it was observed that the system temperature was kept at $\sim$300 K with an acceptable small fluctuation of $\sim$1.1 K.

RESULTS AND DISCUSSION

We first present the effect of the electric field on protein stability by calculating the root mean-square deviation (RMSD),

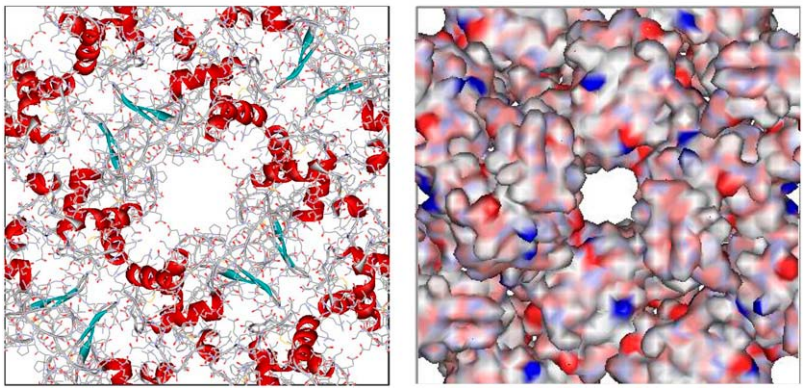

FIGURE 1 A unit cell of tetragonal lysozyme crystal on the *xy* plane. (*a*) Secondary structures: α-helices (*red*), β-sheets (*cyan*), and random coils (*gray*). (*b*) Surface representations of the hydrophobic (*red*) and hydrophilic (*blue*) residues.

the solvent-accessible surface area (SASA), and the number of hydrogen bonds. Then, the structural properties of water and ions are studied, including the dipole moment of water and the number distributions of ions from the protein surface. After these properties are discussed, ion mobility is examined in both crystalline and solution environments, along with the drift velocities of ions, protein, and water. Finally, the electrical conductivity is estimated by extrapolating the current to zero-field limit and comparing it with the prediction from the classical Nernst-Einstein equation.

Protein stability

The stability of protein molecules exposed to an electric field is of importance from a practical point of view. It has been reported that cell membranes exposed to a strong electric field will deform, lose part of surface, or even disintegrate (13). In crystals, lysozyme molecules are constrained at the lattice sites via noncovalent van der Waals and electrostatic interactions and by intermolecular hydrogen bonds. Under the electric field E_z, the positions of lysozyme molecules are shifted to some extent. Fig. 2 *a* shows the averaged RMSDs of lysozyme heavy atoms from the initial crystallographic structure as a function of E_z. The RMSDs increase monotonically with E_z from 0.35 to 0.57 nm upon increasing E_z from 0 to 0.4 V/nm. This finding indicates that the stability of a protein crystal is decreased under the electric field and could cause protein denaturation or damage in the biological functions of protein active sites. Nevertheless, as mentioned above, the electric field used in this study is about one to two orders of magnitude stronger than normally used in experiments to reduce the impact of thermal noise. In reality, the effect of the electric field is substantially less, and protein molecules can maintain their stability fairly well.

TABLE 1 LJ potential parameters and charges

	ε (kJ/mol)	σ (nm)	q (e)
Ca^{2+}	0.507	0.281	+2
Na^{+}	0.062	0.258	+1
Cl^{-}	0.446	0.445	−1
OW	0.650	0.317	−0.82
HW	0	0	+0.41

OW and HW denote the oxygen and hydrogen atoms in the water molecule, respectively.

As shown in Fig. 2 *b*, the hydrophobic SASA increases with E_z and appears to approach a constant at high E_z values, whereas the hydrophilic SASA is essentially independent of E_z. It is recognized that the hydrophobic interaction is one of the major factors involved in protein stabilization (28). Without the electric field applied, the side chains of hydrophobic amino acids are primarily buried inside protein molecules and thus largely inaccessible to solvent. Upon exposure to an external electric field, however, the protein-solvent interface is distorted, and some buried hydrophobic residues become accessible to solvent resulting in a larger SASA. Our results are consistent with an earlier report (29) that suggests protein destabilization in solution is associated with an increase in SASA. Fig. 2 *c* shows the effect of E_z on the numbers of hydrogen bonds between lysozyme molecules and between lysozyme and water molecules, respectively. The intra- and intermolecular hydrogen bonding is a key factor necessary to stabilize a protein crystal. As shown, the external E_z leads to a decrease in the number of hydrogen bonds between lysozyme molecules; in contrast, an increase between lysozyme and water molecules is observed.

Lysozyme consists of several stable structural domains (for example, α-helices and β-sheets), and its stability is well maintained by the intramolecular hydrogen bonds and four disulfide bonds (20,30). The impact of the electric field is further demonstrated by the evolution of lysozyme structures as shown in Fig. 3. In general, the secondary structures including α-helices and β-sheets are well maintained from E_z = 0 to $E_z = 0.4$ V/nm despite some variations. For example, the number of residues (5th to 17th and 25th to 35th residues) forming two α-helices decreases as the electric field increases, implying the partial loss of the secondary structures. Under a strong electric field, a handful of the secondary structures are shifted, and the protein is rearranged somewhat to adopt a favorable conformation.

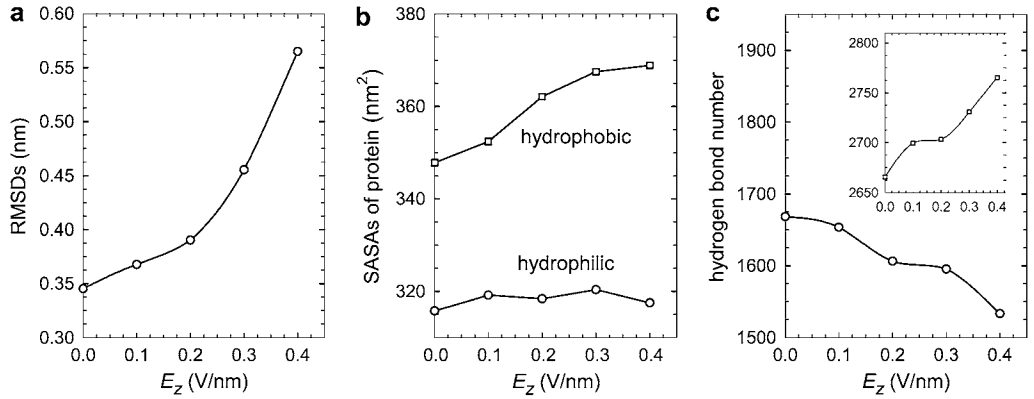

FIGURE 2 (*a*) Averaged RMSDs of lysozyme heavy atoms from the initial crystallographic structure. (*b*) SASAs of hydrophobic and hydrophilic residues. (*c*) Number of hydrogen bonds between lysozyme molecules; the inset shows the number of hydrogen bonds between lysozyme and water molecules.

Two important factors, cross-linking and polarizable charges, were not included in our simulations. Protein crystals are usually cross-linked among each other to enhance the thermal and mechanical stability. The inclusion of cross-linking could practically improve protein stability even at a high electric field. The charges in the GROMOS96 force fields for protein are fixed and not allowed to change. However, the charges could be polarized and vary with the electric field. In future studies, these factors should be taken into account.

Structures of water and ions

Water is a highly polar molecule, and its behavior could be significantly altered upon exposure to an electric field. Recently, Cramer et al. (31) carried out an MD simulation for water adsorbed on a polar surface under an external electric field; their results showed the sudden formation of a water pillar above a threshold field of 1.2 V/nm as a result of the competition between orientational confinement and electric field. In our study, we examined the orientation of the dipole moment of water in the lysozyme crystal. Fig. 4 *a* shows the probability distribution function $P(\theta)$ as a function of angle θ between the dipole moment of water and the z axis. The dipole moment of water is defined by the vector formed from the oxygen atom (OW) to the middle point of two hydrogen atoms (HW) as illustrated in Fig. 4, inset. The probability distribution function $P(\theta)$ was calculated as follows (5):

$$P(\theta) = \frac{\langle \delta N(\theta) \rangle}{\sin\theta} \tag{1}$$

and then normalized by $\sum P(\theta)$ in which $\langle \delta N(\theta) \rangle$ is the ensemble averaged number of water molecules within an angle ranging from $\theta - \delta\theta$ to $\theta + \delta\theta$ ($\delta\theta = 0.5°$ in our calculation).

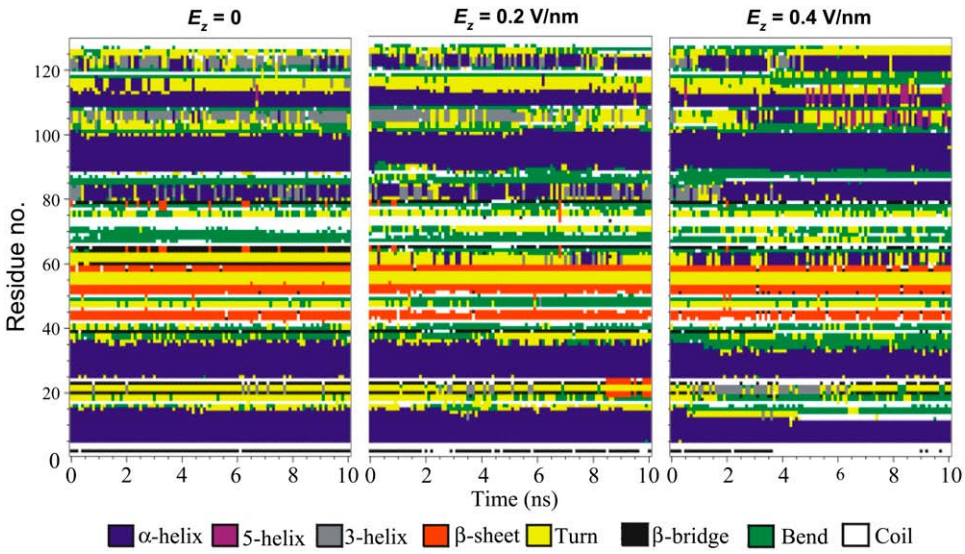

FIGURE 3 Evolution of lysozyme structures as a function of time at three electric fields: $E_z = 0$, 0.2, and 0.4 V/nm, respectively.

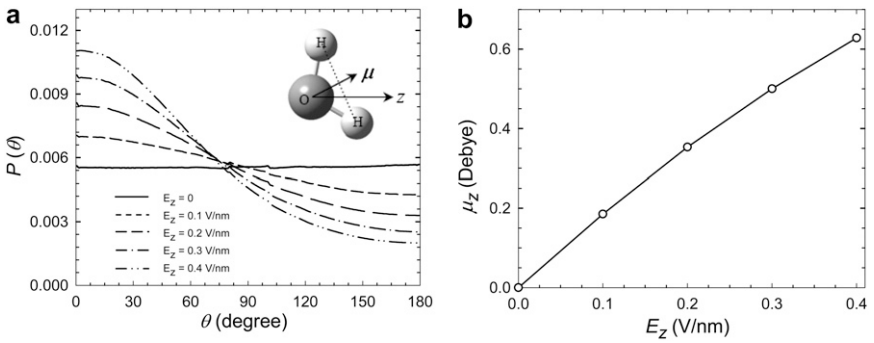

FIGURE 4 (*a*) Probability distribution function of angle θ between the dipole moment of water and the z axis. (*b*) Dipole moment of water along the z axis as a function of the electric field.

At $E_z = 0$ (as derived from the EMD simulation), the dipole moment shows an equally probabilistic distribution at any θ over the range 0–180°. That is, water molecules exhibit a disordered orientation in the complex environment of the lysozyme crystal in which the distribution of nanopores is highly heterogeneous. Upon increasing E_z, $P(\theta)$ starts to exhibit a sigmoid shape with a larger probability at θ between 0 and 90°. This finding implies that the dipole moment tends to orient preferentially along the z axis under the electric field, and the preference becomes more distinct with increasing field strength. A quantitative estimation of the orientation was characterized by calculating the dipole moment directional to the z axis (μ_z). As shown in Fig. 4 *b*, μ_z increases with the electric field strength approximately in a linear fashion. The largest μ_z (at $E_z = 0.4$ V/nm) is ~25% of the dipole moment of simple point charge water molecule (2.27 Debye) (23). The preferred orientation of polar molecules under an electric field may influence the permeation process through protein crystals or biomembranes (32); therefore, the electric field could be used for tuning transport rates.

The binding of a specific ion, also called a cofactor, is essential for the functionality of highly selective catalytic enzymes. It is instructive to examine ion distributions around the protein surface. We calculated the number distributions $N_n(r)$ of Cl^-, Na^+, and Ca^{2+} ions separately as a function of the distance r from the nearest lysozyme atom as follows:

$$N_n(r) = \frac{\langle \delta N(r) \rangle}{N_t \delta r}, \tag{2}$$

where $\langle \delta N(r) \rangle$ is the ensemble averaged number of ions in a layer with thickness of δr ($\delta r = 0.01$ nm in our calculation), and N_t is the total number of ions of each type. The van der Waals radii of protein atoms were taken into account. Note that we did not calculate the density distributions because the volume profile away from the protein surface is difficult to quantify with highly irregular pores or cavities in the crystal structure.

Fig. 5 shows the number distributions at two cases, $E_z = 0$ and 0.4 V/nm. The distributions of all ions are apparently independent of the electric field. Although Cl^- exhibits only one pronounced peak at $r = 0.19$ nm, Ca^{2+} has two peaks at $r = 0.12$ and 0.31 nm; Na^+ also has two peaks at $r = 0.10$ and 0.27 nm. The atomic radii of Ca^{2+}, Na^+, and Cl^- are 0.14, 0.13, and 0.23 nm, respectively (see Table 1), slightly greater than the positions of the first peaks for the three ions. This finding indicates that some ions of each type are closely bound to lysozyme as a result of the electrostatic interactions with the oppositely charged residues in lysozyme. In particular, the first peak of Cl^- (11.4) is much greater than those of Ca^{2+} (3.7) and Na^+ (2.3), because lysozyme is overwhelmingly positively charged and has a significantly stronger affinity to Cl^-. As a rough estimate based on the number distribution profile, ~10% Ca^{2+} or Na^+ cations are located within the first layer, much less than the percentage of Cl^-. Both Ca^{2+} and Na^+ exhibit the second peaks, which are much greater than the first peaks and attributed primarily to their interactions with water molecules. Water forms a hydration layer with a thickness of ~0.3 nm around the protein surface, and there is a minimum in its local density profile at $r \approx 0.3$ nm. Therefore, Ca^{2+} and Na^+ ions can readily intercalate into this less-packed region and show the second peaks at $r \approx 0.3$ nm. Nevertheless, Cl^- has a greater radius compared with Ca^{2+} and Na^+ and thus is largely prohibited from accessing this region. Similar behavior was observed in previous studies of electrolytes in nanopores (33–35).

Fig. 6 shows the water coordination numbers (also called hydration numbers) of three ions and the Cl^- coordination numbers of Ca^{2+} and Na^+ cations as a function of the electric

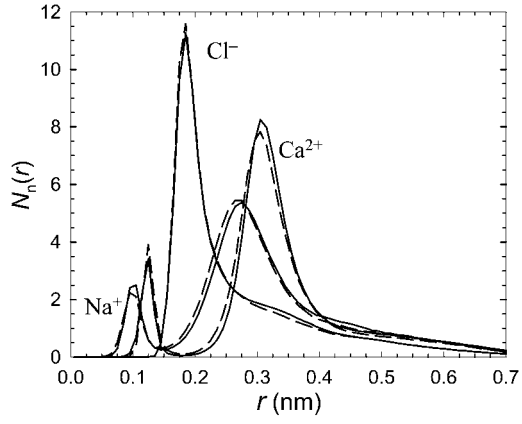

FIGURE 5 Number distributions of ions as a function of the distance from protein surface at $E_z = 0$ (*solid lines*) and $E_z = 0.4$ V/nm (*dashed lines*), respectively.

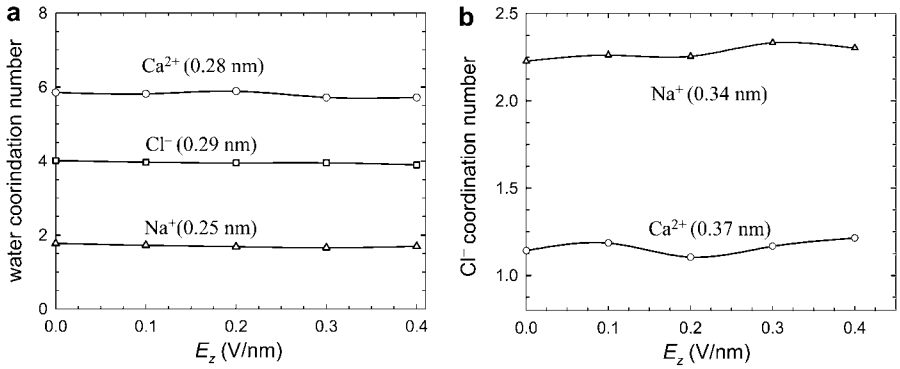

FIGURE 6 (*a*) Water coordination numbers of Ca^{2+}, Na^+, and Cl^-. (*b*) Cl^- coordination numbers of Ca^{2+} and Na^+. The first minimum positions in the radial distribution functions are indicated by the values in parentheses.

field strength. The coordination numbers were estimated by integrating the radial distribution function up to the first minimum position, as indicated in Fig. 6. Both water and Cl^- coordination numbers of ions change marginally with the electric field. This observation is also true for the radial distribution functions between any two species (data not shown), which are nearly independent of the electric field. These structural properties are essentially the *static* not *dynamic* characteristics of the system; thus, they are highly conserved even at a strong electric field. The hydration number of ion is relevant to ionic charge and interaction with water. The bivalent Ca^{2+} strongly interacts with water molecules via the electrostatic and van der Waals interactions; it also has the largest hydration number, whereas Na^+ has the smallest. These findings are also observed for an ion mixture (0.50 M Ca^{2+}, 0.50 M Na^+, and 1.50 M Cl^-) in an aqueous bulk solution, as shown in Table 2, but with larger hydration numbers for all ions. Whereas Cl^- can interact with Ca^{2+} more strongly than with Na^+, the Cl^- coordination number of Na^+ (2.3) is almost twice that of Ca^{2+} (1.2), although this finding seems counterintuitive. Compared to the case in aqueous bulk solution, the Cl^- coordination number is increased in the crystal, particularly for Ca^{2+}. Water and Cl^- interact with Ca^{2+} and Na^+ in a competitive way, and so there is a counterbalance between water and Cl^- coordination numbers. The number of water molecules in the system is overwhelmingly greater than that of Cl^-. Consequently, Ca^{2+} is strongly hydrated by water rather than by Cl^- and so has a weaker interaction with Cl^- compared to the less-hydrated Na^+. Overall, the hydrated Na^+ has a larger Cl^- coordination number than the hydrated Ca^{2+}.

Ion mobility

In the absence of an electric field, ion mobility along the pore axis was examined by calculating the ensemble averaged mean-square displacement (MSD_z) as follows:

$$\mathrm{MSD}_z(t) = \left\langle \frac{1}{N}\sum_{i=1}^{N} |\Delta \mathbf{z}_i(t)|^2 \right\rangle, \quad (3)$$

where t denotes time, N is the number of target particles, and $\Delta \mathbf{z}_i(t)$ is the displacement of molecule i from its initial location in the z axis. The multiple origin method was used to improve the statistical accuracy. Subsequently, the self-diffusivity in the z axis was calculated using the Einstein relation as follows:

$$D_z = \frac{1}{2}\lim_{t\to\infty}\frac{\mathrm{MSD}_z(t)}{t}. \quad (4)$$

Fig. 7 shows the MSDs of the three ions from the EMD simulation. The estimated diffusivities indicated in the parentheses are as follows: 0.018×10^{-9} m^2/s for Ca^{2+}, 0.037×10^{-9} m^2/s for Na^+, and 0.056×10^{-9} m^2/s for Cl^-, which are 2 orders of magnitude smaller compared to the diffusivities in aqueous bulk solution (Table 2). Such a dramatic reduction in the mobility of ions in the lysozyme crystal is attributed to the interaction and steric obstacle of the lysozyme molecules.

Under the electric field, ions are driven to migrate to the nanopore of the lysozyme crystal. At the steady state, each type of ion moves at a constant velocity, referred to as drift or streaming velocity. Fig. 8 shows the effect of the electric field on the drift velocities of the three ions, water, and lysozyme, respectively. The drift velocity was computed by tracking the centers of mass over time. It is known that solvent can migrate in terms of the electroosmotic flow dragged by the ionic stream (36). Nevertheless, in this study, water was found to have a negligible drift velocity due to the electroneutrality of water molecules. On average, the dragging forces from positive and negative ions on water are cancelled out. Lysozyme carrying positive charges exhibits a slight positive displacement, albeit the magnitude is negligible due to the high molecular weight. As expected, Ca^{2+} moves at a positive drift

TABLE 2 Water and Cl^- coordination numbers and self-diffusivities D_z in lysozyme crystal ($E_z = 0$) and in aqueous bulk solution, respectively

	Water coordination No.		Cl^- coordination No.		D_z (10^{-9} m^2/s)	
	In crystal	In solution	In crystal	In solution	In crystal	In solution
Ca^{2+}	5.95	7.67	1.13	0.16	0.018	1.09
Na^+	1.80	3.69	2.24	1.06	0.037	1.13
Cl^-	4.01	6.17	–	–	0.056	1.58

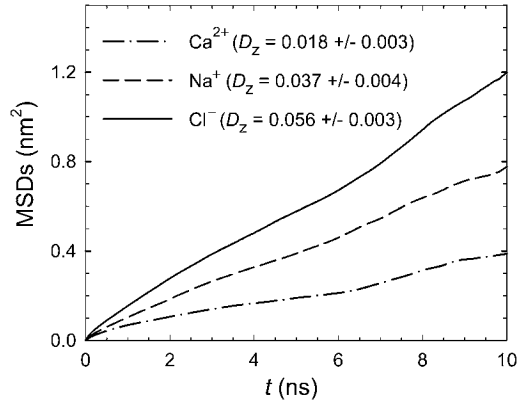

FIGURE 7 MSDs of ions along the z axis from the EMD simulation. The values for estimated self-diffusivities D_z are shown in parentheses with a unit of 10^{-9} m^2/s.

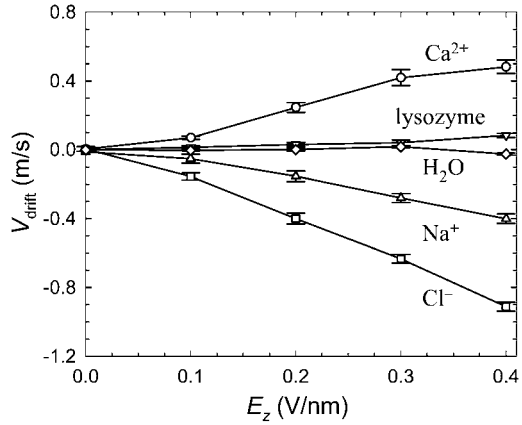

FIGURE 8 Drift velocities of ions, lysozyme, and water along the z axis as a function of the electric field.

velocity, and Cl^- migrates at a negative velocity. See Supplementary Material, Data S1, Movie S1, Movie S2, and Movie S3 for additional information. Interestingly, Na^+, like Cl^-, moves at a negative velocity. The electrophoretic mobility of ions is driven by the external electric field and is affected by the interactions with protein atoms, the hydration states, the dragging and resisting forces of neighboring ions, etc. As a counterbalance to all these complex factors, Cl^- moves at a faster negative velocity under the electric field. The driving force of the electric field and the dragging force of the Cl^- ionic stream create the opposite directions for Na^+ and Ca^{2+}. As shown in Fig. 6 *b*, Na^+ interacts with Cl^- more strongly than Ca^{2+} and has a larger Cl^- coordination number. As a consequence, the Cl^- ionic stream drags Na^+ to flow in a direction that is opposite to that of the electric field. However, Ca^{2+} is compelled by a stronger electrical force than Na^+ and the Cl^- coordination number of Ca^{2+} is smaller; as a result, Ca^{2+} exhibits a positive drift velocity. In other words, the dragging force by the Cl^- ionic stream dominates the electrical force for Na^+, but the reverse is true for Ca^{2+}. Similar phenomenon was observed by Qiao and Aluru (34,35) for an electrolyte mixture in a silicon nanochannel under an electric field in which K^+ and Cl^- migrated in the same direction. In their work, ionic flux was decomposed into two items, namely, an electrical migration component driven directly by the electric field and a convection component dragged by the solvent stream. The strong convection component dominated and resulted in the migration of Cl^- in the reverse direction. In a slightly different manner, our results show that the direction of ion migration can also be reversed by other ions. In our study, the migration of Na^+ is affected by the stream of Cl^-, and thus the former migrates along the direction opposite to the electric field.

Electrical conductivity

Measurement of electrical conductivity in protein crystal is of significance for biosensing and ion exchange techniques. A previous work studied electrical conductivity in a dry lysozyme crystal with orthorhombic symmetry; the results showed an Arrhenius relationship between the conductivity and temperature (37). The movement of trace proton or electron was shown to dominate the conduction process in dry crystal, and the conductivity was found to be very low (10^{-7} to 10^{-9} S/m). In another study, the electrical conductivity was examined for a tetragonal lysozyme crystal immersed in NaCl solution (38). In this case, the conductivity was greatly enhanced to 10^{-2}–10^{-3} S/m compared to that in dry sample.

Electrical conductivity κ can be estimated in two different ways, separately, from EMD and NEMD simulations. In EMD simulations, κ is obtained from the classical Nernst-Einstein equation (39) as follows:

$$\kappa = \frac{e^2}{k_B T}\sum_i D_i \rho_i |q_i|^2 (1-\Delta) = \frac{F_a^2}{RT}\sum_i D_i c_i |q_i|^2 (1-\Delta), \quad (5)$$

where e is the electron charge, T is the absolute temperature, k_B the Boltzmann constant, ρ_i is the number density, c_i is the molar concentration, D_i is the self-diffusivity, q_i is the charge of ith species, and Δ is the cross correlation term that reflects the correlations between different species. F_a is the Farady constant equal to 9.6485×10^4 C/mol, and R is the gas constant. In the Nernst-Einstein equation, conductivity is assumed to be directly proportional to self-diffusivity. The cross-term Δ is usually small and can be reasonably neglected. We then estimated the conductivity in the lysozyme crystal studied here to be 0.61 ± 0.05 S/m.

In the NEMD simulation, the electrical conductivity is obtained from the relationship between the electrical current and the electric field strength. In our study, the current density J_z along the z axis can be expressed as follows (39):

$$J_z = F_a \sum_i c_i q_i v_{i,z}, \quad (6)$$

where $v_{i,z}$ is the velocity along the z axis. Within the linear response range, the zero-field conductivity κ can be extrapolated as follows:

$$\kappa = \lim_{E_z \to 0} \frac{J_z}{E_z}. \quad (7)$$

Fig. 9 shows the current density J_z as the function of the electric field strength. A very good linear relationship is observed in the range of the electric field from our NEMD simulation. The zero-field conductivity κ of the system is estimated as 0.56 ± 0.03 S/m, which is close to 0.61 ± 0.05 S/m within the statistical uncertainty determined from the EMD simulation based on the Nernst-Einstein equation.

CONCLUSIONS

From MD simulations, we have investigated the electrophoretic flow in a tetragonal lysozyme crystal. With increasing electric field strength, the RMSDs of lysozyme atoms are enhanced, more hydrophobic residues are exposed to water, and the secondary structures are slightly destroyed. All these findings indicate that the stability of lysozyme is reduced to some extent by the external electric field. The dipole moment of water in the pore axis increases linearly with the field strength due to the reorientation of water molecules. As a counterbalance between the favorable interaction with protein and the size effect, cations exhibit two pronounced layers around the lysozyme surface, whereas Cl^- has only one enriched layer. The electric field has a negligible effect on the static and structural properties of ions, such as the number distributions and coordination numbers. Compared to aqueous bulk solution, confinement in the crystal remarkably reduces ion mobility. The drift velocities of ions exhibit approximately a linear relationship with the field strength. The movements of Ca^{2+} and Cl^- are primarily dominated by the electric field; nevertheless, the Cl^- ion stream also affects the movement of Na^+ as a consequence of coordination. The electrical conductivity of the system predicted from the NEMD and EMD simulations is in good agreement. The simulation results provide a deeper understanding of the microscopic behavior of protein, water, and ions under the electric field.

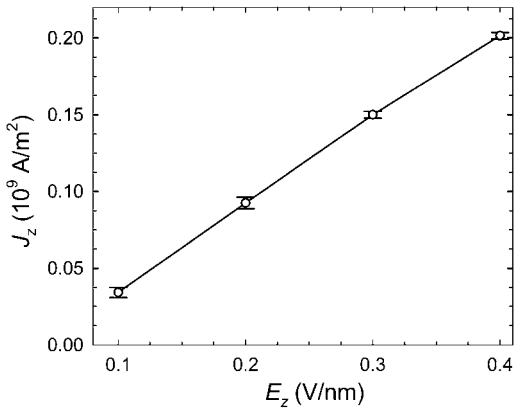

FIGURE 9 Electrical current density along the z axis as a function of the electric field.

This finding is important to elucidate the fundamental mechanism of transport in biomembranes and is useful for the emerging applications of protein crystals as new biosensors and bioseparation media.

SUPPLEMENTARY MATERIAL

To view all of the supplemental files associated with this article, visit www.biophysj.org.

This work was supported by the National University of Singapore (grants R-279-000-198-112/133 and R-279-000-238-112).

REFERENCES

1. Yeung, K. K.-C., and C. A. Lucy. 1999. Ultrahigh-resolution capillary electrophoretic separation with indirect ultraviolet detection: isotopic separation of [14N]- and [15N]ammonium. *Electrophoresis*. 20:2554–2559.
2. Seo, Y. S., H. Luo, V. A. Samuilov, M. H. Rafailovich, J. Sokolov, D. Gersappe, and B. Chu. 2004. DNA electrophoresis on nanopatterned surfaces. *Nano Lett*. 4:659–664.
3. Voet, D., and J. G. Voet. 2004. Biochemistry, 3rd ed. John Wiley & Sons, New York.
4. Jackson, J. D. 1975. Classical Electrodynamics, 2nd ed. John Wiley & Sons, New York.
5. Tang, Y. W., K. Y. Chan, and I. Szalai. 2004. Structural and transport properties of an SPC/E electrolyte in a nanopore. *J. Phys. Chem. B*. 108:18204–18213.
6. Tang, Y. W., I. Szalai, and K. Y. Chan. 2001. Diffusivity and conductivity of a solvent primitive model electrolyte in a nanopore by equilibrium and nonequilibrium molecular dynamics simulations. *J. Phys. Chem. A*. 105:9616–9623.
7. Dzubiella, J., R. J. Allen, and J. P. Hansen. 2004. Electric field-controlled water permeation coupled to ion transport through a nanopore. *J. Chem. Phys*. 120:5001–4.
8. Dzubiella, J., and J. P. Hansen. 2005. Electric field-controlled water and ion permeation of a hydrophobic nanopore. *J. Chem. Phys*. 122: 234706.
9. Murad, S., and J. Lin. 2002. Using thin zeolite membranes and external electric fields to separate supercritical aqueous electrolyte solutions. *Ind. Eng. Chem. Res*. 41:1076–1083.
10. Murad, S., W. Jia, and M. Krishnamurthy. 2004. Ion-exchange of monovalent and bivalent cations with NaA zeolite membranes: a molecular dynamics study. *Mol. Phys*. 102:2103–2112.
11. Hwang, H., G. C. Schatz, and M. A. Ratner. 2006. Ion current calculations based on three dimensional Poisson-Nernst-Planck theory for a cyclic peptide nanotube. *J. Phys. Chem. B*. 110:6999–7008.
12. Hwang, H., G. C. Schatz, and M. A. Ratner. 2007. Kinetic lattice grand canonical Monte Carlo simulation for ion current calculations in a model ion channel system. *J. Chem. Phys*. 127:024706.
13. Dimova, R., K. A. Riske, S. Aranda, N. Bezlyepkina, R. L. Knorr, and R. Lipowsky. 2007. Giant vesicles in electric fields. *Soft Matter*. 3: 817–827.
14. Margolin, A. L., and M. A. Navia. 2001. Protein crystals as novel catalytic materials. *Angew. Chem. Int. Ed*. 40:2205–2222.
15. Vilenchik, L. Z., J. P. Griffith, N. St Clair, M. A. Navia, and A. L. Margolin. 1998. Protein crystals as novel microporous materials. *J. Am. Chem. Soc*. 120:4290–4294.
16. Hu, Z. Q., and J. W. Jiang. 2008. Molecular dynamics simulations for water and ions in protein crystals. *Langmuir*. 24:4215–4223.
17. Evans, D. J., and G. P. Morriss. 1984. Non-Newtonian molecular dynamics. *Comput. Phys. Rep*. 1:297–343.

18. Svishchev, I. M., and P. G. Kusalik. 1993. Dynamic properties of Coulombic systems at low-densities—computer-simulation results. *Physica A*. 192:628–646.

19. Oki, H., Y. Matsuura, H. Komatsu, and A. A. Chernov. 1999. Refined structure of orthorhombic lysozyme crystallized at high temperature: correlation between morphology and intermolecular contacts. *Acta Crystallogr*. 55:114–121.

20. Wilson, K. P., B. A. Malcolm, and B. W. Matthews. 1992. Structural and thermodynamic analysis of compensating mutations within the core of chicken egg-white lysozyme. *J. Biol. Chem.* 267:10842–10849.

21. Kuramitsu, S., and K. Hamaguchi. 1980. Analysis of the acid-base titration curve of hen lysozyme. *J. Biochem*. 87:1215–1219.

22. Schuler, L. D., X. Daura, and W. F. van Gunsteren. 2001. An improved GROMOS96 force field for aliphatic hydrocarbons in the condensed phase. *J. Comput. Chem*. 22:1205–1218.

23. Berendsen, H. J. C., J. P. M. Postma, W. F. van Gunsteren, and J. Herman. 1981. Interaction models for water in relation to protein hydration. *In* Intermolecular Forces. B. Pullman, editor. Reidel, Dordrecht. 331–342.

24. Van der Spoel, D., E. Lindahl, B. Hess, G. Groenhof, A. E. Mark, and H. J. C. Berendsen. 2005. GROMACS: fast, flexible, and free. *J. Comput. Chem*. 26:1701–1718.

25. Pethica, B. A., and D. G. Hall. 1982. Electric-field effects on membranes. *J. Colloid Interface Sci*. 85:41–51.

26. Siu, S. W. I., and R. A. Bockmann. 2007. Electric field effects on membranes: gramicidin A as a test ground. *J. Struct. Biol*. 157:545–556.

27. Tang, Y. W., Q. Y. Zhang, and K. Y. Chan. 2004. Non-equilibrium molecular dynamics simulation of oxygen ion mobility in yttria stabilized zirconia. *Chem. Phys. Lett*. 385:202–207.

28. Dill, K. A. 1990. Dominant forces in protein folding. *Biochemistry*. 29:7133–7155.

29. Collins, K. D. 2004. Ions from the Hofmeister series and osmolytes: effects on proteins in solution and in the crystallization process. *Methods*. 34:300–311.

30. Acharya, A. S., and H. Taniuchi. 1977. Formation of four isomers of hen egg white lysozyme containing three native disulfide bonds and one open disulfide bond. *Proc. Natl. Acad. Sci. USA*. 4:2362–2366.

31. Cramer, T., F. Zerbetto, and R. Garcia. 2008. Molecular mechanism of water bridge buildup. *Langmuir*. 24:6116–6120.

32. Robertson, K. M., and D. P. Tieleman. 2002. Orientation and interactions of dipolar molecules during transport through OmpF porin. *FEBS Lett*. 528:53–57.

33. Freund, J. B. 2002. Electro-osmosis in a nanometer-scale channel studied by atomistic simulation. *J. Chem. Phys*. 116:2194–2200.

34. Qiao, R., and N. R. Aluru. 2003. Ion concentrations and velocity profiles in nanochannel electroosmotic flows. *J. Chem. Phys*. 118:4692–4701.

35. Qiao, R., and N. R. Aluru. 2005. Atomistic simulation of KCl transport in charged silicon nanochannels: interfacial effects. *Coll. Surf*. 267:103–109.

36. Lyklema, J. 1995. Fundamentals of Interface and Colloid Science. Academic Press, San Diego.

37. Ataka, M., and S. Tanaka. 1980. Electrical-conductivity of single-crystals of lysozyme. *Biopolymers*. 19:669–679.

38. Morozova, T. Y., G. S. Kachalova, N. F. Lanina, V. U. Evtodienko, A. S. Botin, E. A. Shlyapnikova, and V. N. Morozov. 1996. Ionic conductivity, transference numbers, composition and mobility of ions in cross-linked lysozyme crystals. *Biophys. Chem*. 60:1–16.

39. Plawsky, J. L. 2001. Transport Phenomena Fundamentals (Chemical Industries). Marcel Dekker, New York.